A Collaborative Robotic Platform for Sensor-Aware Fibula Osteotomies in Mandibular Reconstruction Surgery

Junlei Hu (junleihuman@gmail.com)
Shanghai Jiao Tong University School of Medicine Affiliated Ninth People's Hospital
https://orcid.org/0000-0001-7394-5580

Jiannan Liu
Shanghai Jiao Tong University School of Medicine Affiliated Ninth People's Hospital

Yan Guo
Shanghai Jiao Tong University School of Mechanical Engineering

Zhenggang Cao
Shanghai Jiao Tong University

Xiaojun Chen
Shanghai Jiao Tong University School of Mechanical Engineering https://orcid.org/0000-0002-0298-4491

Chenping Zhang
Shanghai Red Cross Ninth People's Hospital: Shanghai Jiao Tong University School of Medicine Affiliated Ninth People's Hospital

---

Research Article

Keywords: Mandibular reconstruction with free fibula flap, Surgical robot, sensor-aware fibula osteotomy, Physical human-robot interaction

Posted Date: October 19th, 2022

DOI: https://doi.org/10.21203/rs.3.rs-2105517/v1

A Collaborative Robotic Platform for Sensor-Aware Fibula Osteotomies in Mandibular Reconstruction Surgery

Junlei Hu[1,2†], Jiannan Liu[1*†], Yan Guo[2], Zhenggang Cao[3], Xiaojun Chen[2,3*] and Chenping Zhang[1*]

[1*]Department of Oral Maxillofacial - Head & Neck Oncology, Shanghai Ninth People's Hospital Affiliated to Shanghai Jiao Tong University School of Medicine, 200011, Shanghai, China.
[2]School of Mechanical Engineering, Shanghai Jiao Tong University, 200240, Shanghai, China.
[3]Institute of Medical Robot, Shanghai Jiao Tong University, 200240, Shanghai, China.

*Corresponding author(s). E-mail(s): laurenceljn@163.com; xiaojunchen@sjtu.edu.cn; zhang.chenping@hotmail.com;
Contributing authors: junleihuman@gmail.com; yan_guo@sjtu.edu.cn; caozg_001@sjtu.edu.cn;
†These authors contributed equally to this work.

Abstract

Fibula osteotomy needs to be performed precisely and safely in mandibular reconstruction with free fibula flap (FFF). However, current clinical methods, such as template-guided osteotomy, have potential for damage to fibular vessels. To address the challenge, this paper introduces the development of the surgical robot for fibula osteotomies in mandibular reconstruction surgery and propose an algorithm for sensor-aware hybrid force-motion control for safe osteotomy, which includes three parts: osteotomy motion modeling from surgeons' demonstrations, Dynamic-system-based admittance control and osteotomy sawed-through detection. As a result, the average linear variation of the osteotomized segments was $\mathbf{1.08 \pm 0.41}$ mm, and the average angular variation was $\mathbf{1.32 \pm 0.65^\circ}$. The threshold of osteotomy sawed-through detection is **0.5** at which the average offset is **0.5**mm. In conclusion, with the assistance of surgical robot for mandibular reconstruction, surgeons can perform fibula osteotomy precisely and safely.

Keywords: Mandibular reconstruction with free fibula flap, Surgical robot, sensor-aware fibula osteotomy, Physical human-robot interaction

1 Introduction

The use of free vascularized fibula has become the "gold standard" for mandibular reconstruction after tumor ablation. [1] The flaps should be modeled with multiple osteotomies because of the non-linear nature of the mandibular bone. The precise preoperative planning and intraoperative osteotomies are of vital importance to ensure correct bone-to-bone contact, and maxillo-mandibular and occlusal relationships, because imprecise operation will ultimately lead to a higher rate of complications and poor aesthetic and functional results. Most importantly, peroneal artery and vein closed to fibula (about 5mm) are supposed to be intact while osteotomy because they need to be anastomosed to the recipient vessels to maintain endosteal circulation.

Computer-assisted mandibular reconstruction (CAMR) has further increased the accuracy of preoperative planning, resulting in greater precision of the surgical procedure [2]. CAMR requires careful planning in order to obtain the best oncological, functional and aesthetic outcome. The surgical template to guide fibula graft osteotomy have been applied in clinic [3–8]. It is designed to conform to the surface of fibula, and three-dimensional (3D) printed with bio-compatible materials. However, surgical template has the drawback of a limited intraoperative flexibility, leading to have some safety risk, e.g., the margin of mandible tumor cannot be perfectly determined before the intraoperative pathologic analysis; the the resection margins are much larger than planned before and virtual surgical planning (VSP) therefore fails. Besides, the deformation of template or imperfect fit will also cause inaccuracies. The key shortage of surgical template in mandibular reconstruction is that the osteotomy depth is hard to control, leading to damage on peroneal artery or vein, because surgeons have to cut fibula in considerable force (above 10N) and suffer high-frequency oscillation.

Image-guided surgical robot is an alternative to oral and maxillofacial surgery [9], which can precisely and steadily positioning on the osteotomy planes according to the preoperative planning. There are several surgical robot systems for mandibular reconstruction. For example, the research group from Beijing Institute of Technology developed a master-slave robot system used for positioning implant on defected mandible [10, 11]. Chao *et al.* investigate the feasibility and accuracy of performing osteotomies robotically in preprogrammed fashion for mandibular reconstruction with FFF as a method to reduce inaccuracies related to human error [12]. Augello *et al.* [13, 14] developed a robotic-assisted laser-osteotomy system for mandibular reconstruction.

The Er:YAG laser was guided by the optical tracking system to osteotomy. Haptic virtual fixtures were used to guide fibulectomies with two kinds of robots [15, 16]. However, during the osteotomy, surgeons are unable to have physical interaction with robot. Collaboration between a surgeon and robot combines the mental abilities of a surgeon and the electromechanical abilities of a robot. As automated osteotomy by robot is yet not clinically available, dependency on the surgeon-in-the-loop surgery imposes demand for user control strategy such that the surgeon could master robot directly at his/her discretion. Under the haptic guidance, surgeons can focus on their hands and patient rather than the monitor.

Although the surgical saw can be located to the cutting plane with the help of robot, the peroneal vessels may be at risk during robot-assisted fibulectomy because of the limited positional accuracy. It was reported that the linear variation of the osteotomized segments was 3.7 ± 2.0mm in haptic guidance [15] and 1.36 ± 0.4mm in medical image guidance [17]. Open-loop or position-based control may not be sufficient for safe fibulectomy, but cutting force can indicate the termination of osteotomy because a sudden drop-off in cutting force can be observed when the blade passes through the fibula. Another problem is the safety of robot controlling because robot-assisted osteotomy is a contact task with stiff environments. For example, if the saw was turned off while the robot was still going downward, the force would increase dramatically, making the fibula unsteady; the irregular shape of fibula may result in an incomplete osteotomy. Surgical robot with precise force sensor and quick-reaction can terminate osteotomy. Several works have sought to develop safe and auto robotic operation on hard tissues without damaging the vessels in craniotomy [18]. However, there has been no detailed investigation of hybrid force-position control for robot in fibulectomy.

With the integration of more sensors, higher level of surgical robot autonomy may become realized [19]. Fibula osteotomy, the sub-tasks in mandible reconstruction, has the potential to be more autonomous because it is operated extracorporeally. The aforementioned system [10, 12, 13] are in the level of teleoperation or programmed-execution, according to [20]. The perception of fibula osteotomy has not been fully study.

There are two primary contributions of this study:

- The collaborative surgical robot system with the novel fibula holder for mandibular reconstruction is presented. Combining image- and haptic-guidance, fibula osteotomy can be performed easily and precisely.
- The sensor-aware robotic osteotomy, learned from demonstrations of experts, is a brand-new method for robotic manipulation with hard tissues. The online force-motion controller with safety intervention can adjust to different shapes of fibula as well as disturbances on surgical instrument.

The remainder of this paper is organized as follows. Section 2 describe the hardware and workflow of the surgical robot system for mandibular reconstruction, as well as the hybrid force-motion control for fibular osteotomy. Section

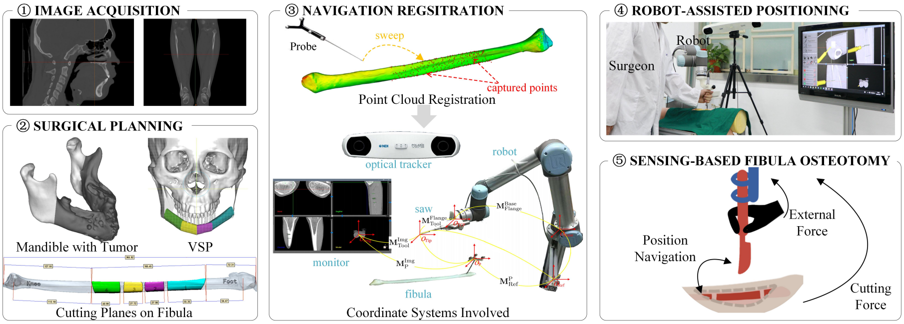

Fig. 1 Workflow of surgical robot for fibula osteotomy in mandibular reconstruction with FFF

3 gives the description about data acquisitions and the experiments carried out with the surgical robot system. Finally, in section 5, the discussion and conclusion are drawn.

2 Methodology

2.1 Workflow

The workflow of robot-assisted surgery for fibula osteotomies in mandibular reconstruction is shown in Figure 1, the details of every component is illustrated as follows:

2.1.1 Image acquisition

The preoperative computerized tomography (CT) scan of the patient's craniofacial skeleton and angiographic CT scan of lower extremities will be taken for 3D reconstruction, surgical planning, and registration.

2.1.2 Virtual surgical planning

The amount of FFFs, the side of lower extremity and the type of reconstruction are determined according to the shape of the mandibular defect [21]. The shaping and placement of FFFs are planned by simulating on the 3D virtual model of defected mandible reconstructed from the CT image data. Then, the desired path of the surgical saw could be obtained from the VSP.

2.1.3 Navigation registration

The steps of registering fibula in real world to virtual model under optical navigation are initial alignment and refinement.

In the stage of initial alignment, the fibula holder with reflecting markers can be located by the optical tracker. In addition, because the fibular segment was fixed on the fibula holder, their spatial relationship can be estimated according to the mechanical parameters. Therefore, the initial guess of the registration matrix can be computed.

The refinement was achieved by means of registering the point cloud recorded by sweeping the probe on the surface of fibula to the surface, as shown in Figure 1.

2.1.4 Robot-assisted positioning

After intraoperative navigation registration, the robot can precisely implement VSP on the real fibula according to the relationship:

$$\mathbf{M}_{\mathrm{Tool}}^{\mathrm{Img}} = \mathbf{M}_{\mathrm{P}}^{\mathrm{Img}} \cdot \mathbf{M}_{\mathrm{Ref}}^{\mathrm{P}} \cdot \mathbf{M}_{\mathrm{Base}}^{\mathrm{Ref}} \cdot \mathbf{M}_{\mathrm{Flange}}^{\mathrm{Base}} \cdot \mathbf{M}_{\mathrm{Tool}}^{\mathrm{Flange}} \tag{1}$$

where $\mathbf{M}_{\mathrm{Flange}}^{\mathrm{Base}}$ is the rigid transformation of end-effector frames with respect to robot base frames, which can be computed through forward kinematics; $\mathbf{M}_{\mathrm{Ref}}^{\mathrm{P}}$ is the transformation between the reference frames of patient and robot, was determined in the stage of navigation registration; $\mathbf{M}_{\mathrm{Tool}}^{\mathrm{Flange}}$ is the tool-flange matrix and $\mathbf{M}_{\mathrm{Base}}^{\mathrm{Ref}}$ equals robot-world matrix. $\mathbf{M}_{\mathrm{Tool}}^{\mathrm{Flange}}$ and $\mathbf{M}_{\mathrm{Base}}^{\mathrm{Ref}}$ are calibrated [22].

In the procedure of positioning, robot is forced to interact with surgeon according to the following desired behavior:

$$\mathbf{M}\ddot{\mathbf{x}} + \mathbf{B}\dot{\mathbf{x}} = \mathbf{F}_{\mathrm{S}} \tag{2}$$

where $\mathbf{M} \in \mathbb{R}^{6\times6}$ and $\mathbf{B} \in \mathbb{R}^{6\times6}$ are inertia and damping symmetric and positive-definite matrices, $\mathbf{x} \in \mathbb{R}^6$ is the pose of the end-effector. The external force $\mathbf{F}_{\mathrm{S}}$ is assumed to be measured by the F/T sensor.

In order to guide the robot to the position of the active cutting plane through haptic, the velocity in some dimensions of the blade was constrained like:

$$\widetilde{\mathbf{V}} = \mathrm{diag}\{\alpha_1, \alpha_2, 1, \alpha_4, \alpha_5, 1\}\dot{\mathbf{x}} \tag{3}$$

where $\alpha_i \in [0,1]\,(i = 1,2,4,5)$ is the constraint coefficient relative to the deviation between real and desired position, and $\widetilde{\mathbf{V}}$ is the constrained speed, making it difficult for surgeon to overpower tactile forces on the end-effector and guide the blade in the incorrect direction.

2.1.5 Osteotomies

When the blade reaches the entry of planned trajectories, the osteotomy is started. During the procedure, robotic osteotomy will be performed under optical navigation with VSP, but surgeons can take control over the robot system by directly lifting or dropping the osteotomy saw and respond to emergencies. The 6-axis force sensor at the end-effector will monitor the external force, then the robot system will react to surgeon's action. In addition, the force sensor on the fibula holder measures the cutting force over time. Once the cutting force drops below the threshold which balances osteotomy success and safety, the

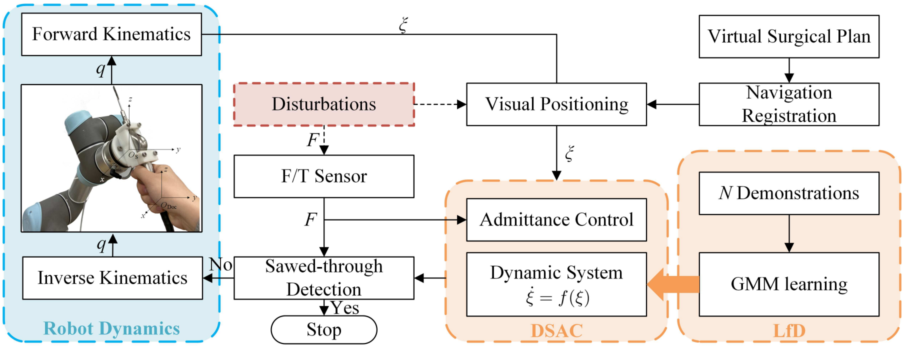

Fig. 2 Illustration of the control flow of robotic system for sensor-aware fibula osteotomy. The main architecture is the hybrid force-motion control for fibula osteotomy, including osteotomy motion modeling from N demonstrations, DSAC and the sawed-through detection algorithm.q refer to the joints of robot, LfD is short for learning from demonstration

motion will be halted to avoid destroy on fibular vessels. The detailed control for osteotomy is delineated in Section 2.2.

2.2 Sensor-aware Fibular Osteotomy

Surgical robot may suffer from various disturbance during the osteotomy, such as sudden displacement of fibula segment,external force introduced by human interactions. To address this problem, the dynamics system was introduced for real-time robot motion planning. Dynamics system have been advocated as a powerful alternative to modeling robot motions which takes as input a state variable $\xi \in \mathbb{R}^3$ and returns the rate of change of that variable:

$$\dot{\xi} = f(\xi) \tag{4}$$

The dynamic system can be learned from a set of demonstrations, and the function f describes all possible solutions to target. However, apart from the perturbation, robot has to react to force disturbance from either sawing or human during osteotomy. Admittance control was offered as a solution to some of these drawbacks. Therefore, the sensor-aware fibula osteotomy includes three parts: osteotomy motion modeling, dynamic-system-based admittance control (DSAC) and sawing-through detection (Figure 2). The osteotomy motion models were learned from multiple demonstrations of the task. The sawed-through detection algorithm was used to stop the osteotomy

2.2.1 Osteotomy Motion Modeling

The purpose of osteotomy motion modeling is to generate a stable dynamical system where the motion is uniquely determines by the state ξ. For robot-assisted fibulectomy, the practical solution to encode a trajectory is taking as input the position and as output the velocity, because the accelerate of end-effort is hard to be measured for many robotic systems and the derivative of the velocity is noisy. Thus, ξ represents the position of blade in our study. To model the motion in fibulectomy, a set of demonstrations of experienced surgeons were adopted. The position and the speed of blade relative to fibula were recorded in each demonstration.

Estimating f is learned from N demonstrations. In order to create a probabilistic representation of the temporally aligned phase data that were obtained from the demonstrations, a Gaussian Mixture Model (GMM) was used. For a data set represented by x_j a K-components GMM is defined by the following probability density function:

$$
\begin{aligned}
P\left(\xi_j, \dot{\xi}_j\right) &= \sum_{k=1}^{K} \phi_k \mathcal{N}\left(\xi_j, \dot{\xi}_j;\ \mu_k, \Sigma_k\right) \\
\mathcal{N}\left(\xi_j, \dot{\xi}_j;\ \mu_k, \Sigma_k\right) &= \frac{1}{\sqrt{(2\pi)^K |\Sigma_k|}} \mathrm{e}^{-\frac{1}{2}(\Xi_j-\mu_k)^{\mathrm{T}}\Sigma_k^{-1}(\Xi_j-\mu_k)} \\
\Xi &= \left[\xi, \dot{\xi}\right]
\end{aligned}
\tag{5}
$$

where $\{\xi_j, \dot{\xi}_j\}$, for $j = 1, \ldots, N$,is a data point of one demonstration, ϕ_k is the mixing weight of each Gaussian g_i with the constraint that $\sum_{k=1}^{K} \phi_k = 1$, $\mu_k = \begin{bmatrix} \mu_{\xi,k} \\ \mu_{\dot{\xi},k} \end{bmatrix}$ and $\Sigma_k = \begin{bmatrix} \sigma^2_{\xi,k} & \sigma_{\xi\dot{\xi},k} \\ \sigma_{\xi\dot{\xi},k} & \sigma^2_{\dot{\xi},k} \end{bmatrix}$ are the estimated means and covariances of g_i respectively.

The conditional expectation of $\dot{\xi}_i$, for $i = 1, \ldots, K$, in each Gaussian g_i is

$$
\hat{\dot{\xi}}_i = \mu_{\dot{\xi},i} + \frac{\sigma_{\xi\dot{\xi},i}}{\sigma^2_{\xi,i}} \left(\xi - \mu_{\xi,i}\right) \tag{6}
$$

Then, for input the state ξ, the conditional expectation $\dot{\xi}$ of the resulting mixture may be written as [23]

$$
\hat{\dot{\xi}} = \sum_{k=1}^{K} h_k(\xi) \hat{\dot{\xi}}_k \tag{7}
$$

where $h_k(\xi) = \frac{P(k)P(\xi|k)}{\sum_{i=1}^{K} P(i)P(\xi|i)}$ is a state-dependent mixing function, according to the stable estimator of dynamical systems (SEDS) approach [24]. The approximating $f(\xi)$ as a non-linear combination (or mixture) of linear dynamic system.

2.2.2 Dynamic-system-based Admittance Control

When the model of osteotomy motion is established, robot can adjust its trajectory and speed immediately according to real-time position. Before contacting with the fibula, the desired and nominal dynamic system is aligned and identical. However, in process of osteotomy, the blade always cannot move at the

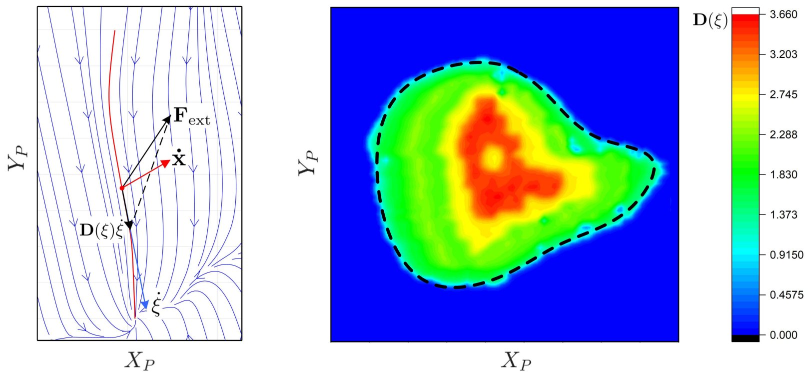

Fig. 3 (a) Illustration of DSAC, the blue arrows represent the field of velocity, X_P and Y_P are the $X-$ and $Y-$axis of patient frame. (b) The disturbance of the force threshold $D(\xi)$, the black dash line indicates the outer boundary of fibula section

desired speed generated from the motion model due to the obstruction of hard tissue, then the cutting force will increase dramatically. Thus, admittance control was introduced to convert the external force to the motion of osteotomy saw. As a result, the robot is supposed to move according to the combined motion. During the osteotomy, the admittance control in (2) will be extended as

$$\mathbf{M}\left(\ddot{\mathbf{x}}-\ddot{\xi}\right)+\mathbf{B}\left(\dot{\mathbf{x}}-\dot{\xi}\right)+\mathbf{K}\left(\mathbf{x}-\xi\right)=\mathbf{F}_{\text{ext}}-\mathbf{D}(\xi)\dot{\xi} \tag{8}$$

where $\left(\xi,\dot{\xi}\right)$ is the current state; $\mathbf{K}$ is stiffness matrix to be simulated by the robot, $\mathbf{F}_{\text{ext}}$ is the external force. The $\mathbf{M}$ and $\mathbf{B}$ has the same value as Eq.(2) for smooth transition in different stages. The solvers of this and Eq.(2) are traditional admittance controller.

In our study, the admittance control will not react to the external force lower than the threshold $\mathbf{D}(\xi)\dot{\xi}$. $\mathbf{D}(\xi) \in \mathbb{R}^{6\times 6}$ is a state-varying damping matrix. As shown in Figure 3(b), the $\mathbf{D}(\xi)=0$ when the blade not contact with the fibula, and it increases in area with higher bone mineral density (BMD). The correlation between the Hounsfield Units(HU) measurement and BMD has been firmly established [25].

2.2.3 Fibula Sawed-through Detection Algorithm

When the blade touches or passes through the fibula, there will be a stereotyped increase or decrease in force. Thus, we developed an algorithm based on this information as well as the fibular diameter to detect fibula split-down. Fibular diameter, the distance between the entry and exit point of planned trajectory, can be obtained from VSP, as shown in Figure 4(a).

To find the threshold that resulted in the smallest excess of the blade when the osteotomy finishes, a set of demonstrations were carried out and measured

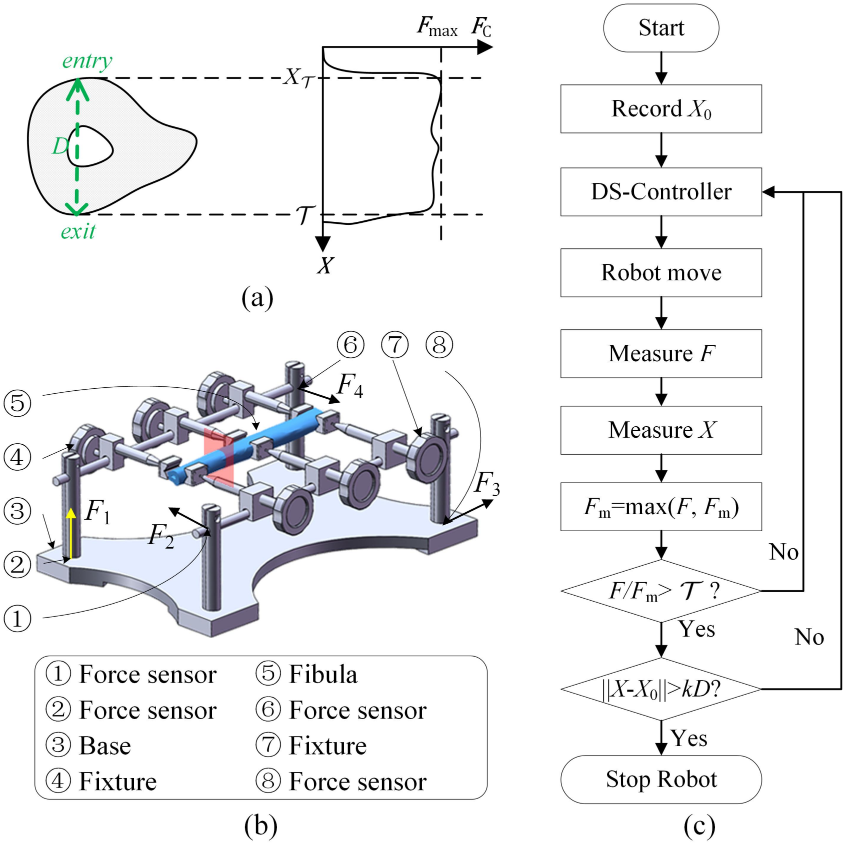

Fig. 4 a) Illustration of the sawed-through detection, section of fibula and the curve of cutting force. (b) A new fibula holder with four force sensors. The cutting force in the osteotomy plane(red) can be obtained through the fusion of force data. The number of pairs of fixtures is determined by VSP. (c) Flowchart of Sawed-through detection algorithm.

the force. For each trial, the terminal position of osteotomy is defined as

$$X_{\mathcal{T}} = \arg\min_{X} \left(\int_{0}^{X} F(x)\mathrm{d}x + \int_{X+D}^{\infty} F(x)\mathrm{d}x \right) \tag{9}$$

where $F(\bullet)$ denotes the collected force-position function, and D is the fibular diameter in that section. The aim is to minimizing the energy not used for osteotomy.

Thus, the normalized terminal threshold is

$$\mathcal{T} = \frac{F(X_{\mathcal{T}} + D)}{F_{\max}} \tag{10}$$

where $F_{\max}$ is the maximum force in that trail. The general threshold $\mathcal{T}$ be defined that balanced osteotomy success and safety. In the procedure of osteotomy, the force curve is supposed to be recorded, and the start and termination can be detected according to maximum force multiplies threshold.

The data of F/T sensor will be affected by the external force when hold by surgeons. In order to precisely measure the cutting force, four force sensors (strain gauges) at different directions (F_1, F_2 and F_3 are all orthogonal, F_2 and F_4 are opposite) were integrated on the fibula holder, as shown in Figure 4(b). During the osteotomy, both the fibula and holder are assumed to be static and the forces are in equilibrium, thus the cutting force is

$$F_C = -\sum_{i=1}^{4} F_i \tag{11}$$

where F_i is the force of No.i sensor after load compensation.

The control flow was illustrated in the Figure 4(c). The force and position are recorded to monitor the osteotomy.

3 Results

3.1 Experimental Setup

As shown in Figure 5, the main body of the surgical robot system is the 6-DoF (degree of freedom) articulated manipulator (UR5; Universal Robot, Odense, Denmark). A 6-axis force torque (F/T) sensor (OnRobot, Odense, Denmark, measuring range ±145N on X-Y plane, ±290N on Z axis, ±5Nm on all axes, resolution 1/16N - 1/752Nm) was attached at the robot wrist flange to measure the force and torque during human-robot interaction or osteotomy. The reciprocating surgical saw (Aesculap AG, Tuttlingen, German) was fixed on the F/T sensor using a customized attachment and could be driven by the pedal. The fibula holder was used to fix the fibula segments during the surgery. An optical tracking system (Polaris; Northern Digital Inc., Waterloo, Canada) was used to capture the realtime poses, including position and orientation, of the manipulator and the fibula with the dynamic reference frames that were rigidly attached to the robot base and fibula. And the main center was a workstation for surgical planning, real-time display and robot control.

With the approval of Ethics Committee of Shanghai Ninth People's Hospital, Shanghai Jiao Tong University School of Medicine, three cases of mandibular reconstruction with four-segments FFF were adopted. Resin-based phantoms of fibula were 3D-printed according to their CT scans. A mock peroneal artery and vein were added to the model using electrical wiring. VSP was conducted by the experienced surgeon on the intelligent planing system developed by our group then loaded to the surgical robot software.

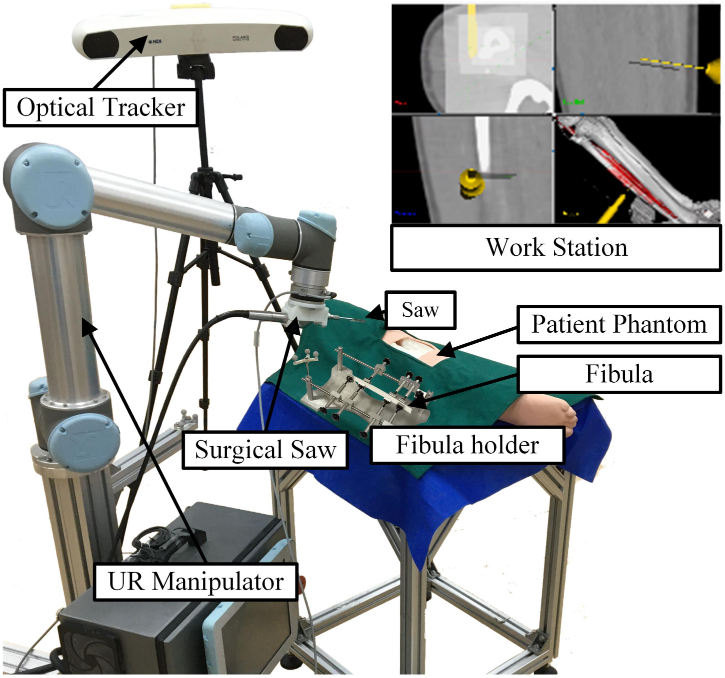

Fig. 5 Hardware of robot for fibulectomy in mandibular reconstruction.

3.2 Data Acquisitions

For collection of demonstration data (including motion, force and virtual osteotomy plane), a platform consisting the same devices as robot system was established for this study. As shown in the Figure 6, a fixture rigidly connected the fibula model and the F/T sensor mounted on the desktop. Surgeon can cut the fibula with osteotomy saw free hand. During the operation, both the fibula model and the osteotomy saw can be located by the optical tracker. The surgical saw was calibrated and the fibula model was registered preoperatively. Thus the real-time relative pose between blade and fibula, denoted as $\mathbf{M}_{\mathrm{Tool}}^{\mathrm{P}} \in SE(3)$, can be computed through matrix chain.

In order to collect real-time velocity and smooth the data for osteotomy motion modeling, the Extended Kalman Filter (EKF) [26] in vector space of Lie algebra $\mathfrak{se}(3)$ was used. The pose and velocity of the blade relative to fibula in 6-dimensional vector space are $\xi = \begin{bmatrix}\boldsymbol{\rho}^{\mathrm{T}} & \boldsymbol{\phi}^{\mathrm{T}}\end{bmatrix}^{\mathrm{T}}$ and $\dot{\xi} = \begin{bmatrix}\boldsymbol{v}^{\mathrm{T}} & \boldsymbol{\omega}^{\mathrm{T}}\end{bmatrix}^{\mathrm{T}}$ respectively. The form of the discrete time state space model for the state $\mathbf{x} = \begin{bmatrix}\boldsymbol{\rho}^{\mathrm{T}} & \boldsymbol{\phi}^{\mathrm{T}} & \boldsymbol{v}^{\mathrm{T}} & \boldsymbol{\omega}^{\mathrm{T}} & \dot{\boldsymbol{v}}^{\mathrm{T}} & \dot{\boldsymbol{\omega}}^{\mathrm{T}}\end{bmatrix}^{\mathrm{T}}$ and the measure $\mathbf{y} = \begin{bmatrix}\boldsymbol{\rho}^{\mathrm{T}} & \boldsymbol{\phi}^{\mathrm{T}}\end{bmatrix}^{\mathrm{T}}$ is

$$\begin{aligned} \mathbf{x}_{k+1} &= \mathbf{f}(\mathbf{x}_k) + \mathbf{w}_k \\ \mathbf{y}_k &= \mathbf{C}\mathbf{x}_k + \boldsymbol{\nu}_k \end{aligned} \tag{12}$$

where k is the current time step, $\mathbf{C} = [\mathbf{I}_{6\times 6} \quad \mathbf{0}_{6\times 12}]$, $\mathbf{w}_k$ is the process noise and $\boldsymbol{\nu}_k$ is the measurement noise. The nonlinear state-transition function is

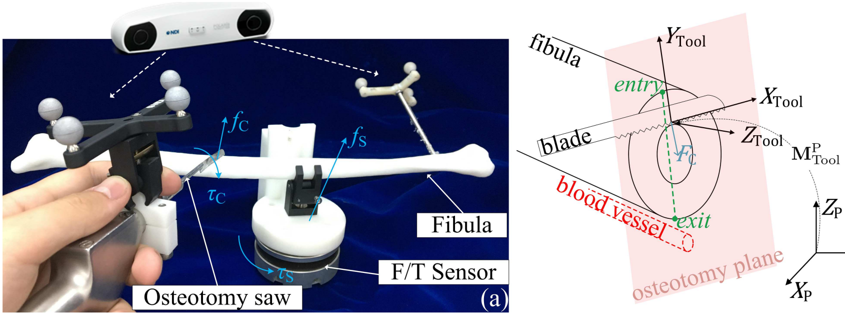

Fig. 6 (a)The platform for collecting osteotomy data. (b) The illustration of acquired motion and force information. The green dash line represents the planned trajectory within osteotomy plane.

defined as

$$\mathbf{f}\left(\mathbf{x}_k\right) = \begin{bmatrix} \boldsymbol{\rho}_k + v\Delta t + \frac{1}{2}\dot{\boldsymbol{v}}_k \Delta t^2 \\ \log\left(\boldsymbol{\phi}_k^\wedge(\boldsymbol{\omega}_k^\wedge \Delta t + \frac{1}{2}\dot{\boldsymbol{\omega}}_k^\wedge \Delta t^2 + \mathbf{I}_3)\right)^\vee \\ \boldsymbol{v}_k + \dot{\boldsymbol{v}}_k \Delta t \\ \boldsymbol{\omega}_k + \dot{\boldsymbol{\omega}}_k \Delta t \\ \dot{\boldsymbol{v}}_k \\ \dot{\boldsymbol{\omega}}_k \end{bmatrix} \tag{13}$$

where Δt is is the sample time, $[\bullet]^\wedge$ is the vector of skew-symmetric matrix, and $[\bullet]^\wedge$ is the skew-symmetric matrix of a vector.

In the meantime, the cutting force in demonstration was recorded as well. Before osteotomy, the force and torque should be set to zero to compensate the load. During the operation, fibula can be regarded to be at rest, and there was no external force for the system except cutting force. Thus, the cutting force

$$\mathbf{F}_\mathrm{C} = -\begin{bmatrix} \mathbf{I}_3 & 0 \\ \mathbf{t}_\mathrm{P}^{\mathrm{Tool}\wedge} & \mathbf{I}_3 \end{bmatrix} \mathbf{F}_\mathrm{S} \tag{14}$$

where $\mathbf{F}_\mathrm{S} \in \mathbb{R}^6$ is the data of the F/T sensor, $\mathbf{t}_\mathrm{P}^{\mathrm{Tool}} \in \mathbb{R}^3$ is the translation vector between balde and patient (fibula model), $\mathbf{I}_3$ is the 3×3 identity matrix.

Osteotomy on phantom by hand was performed 12 times with each of the trajectories learned from the two experience levels, across four inexperienced operators. The approach to minimize the impact of reciprocating is projecting the $\mathbf{F}_\mathrm{C}$ on the osteotomy line, as shown in Figure 6. In addition, the motion of blade relative to fibula can be simplified to be two-dimensional because the lateral movement can be omitted.

3.3 Fibula Segment Measurements

One expert operator and two intermediate level operators respectively completed 8 fibula osteotomies on each fibula models with surgical robot. Each fibula should be osteotomied for 8 times to obtain 4 FFFs. In navigation registration, the mean error of the ICP algorithm was 0.78 ± 0.46mm. Then,

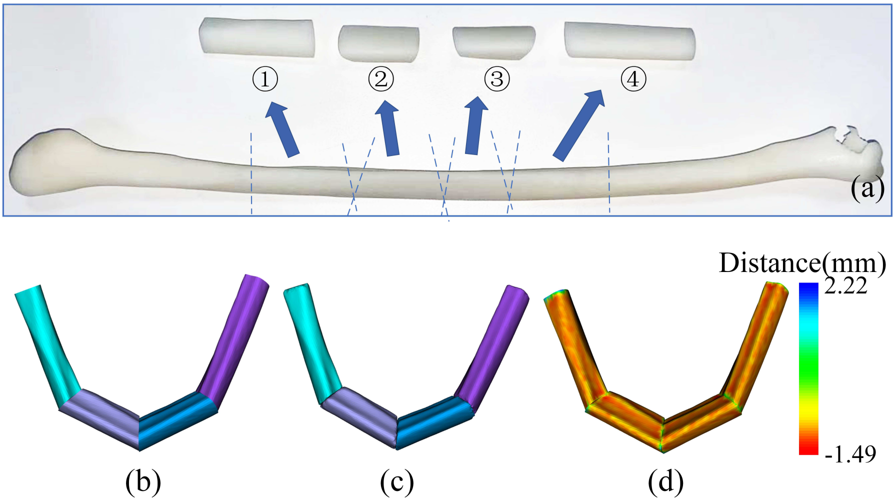

Fig. 7 (a) Four FFFs were harvested from one fibula resin phantom sequentially. The blue dash lines indicated the osteotomy planes. (b) The pre-operative planning for mandibular reconstruction with FFF. (c) Each FFF was reconstructed from post-operative CT scanning and registered to the corresponding one in (b). (d) The color map indicating the the registration error between pre- and post-operative 3D reconstructed FFFs.

postoperative CT scanning of the harvested FFFs was performed with the same scanner to evaluate the accuracy of robot-assisted osteotomy. Two primary outcome measures were then utilized: fibula segment length variation and osteotomy angle variation.

Each FFF was segmented and reconstructed from postoperative CT images (slice thickness of 0.50mm and an average in-plane resolution of 0.39mm/pixel) through the open source software — 3D Slicer (https://slicer.org), and the resultant 3D digital models then superimposed on the fibula segments from the preoperative surgical planning, as shown in Figure 7. A total of 72 osteotomies were performed on nine 3D printed fibula phantoms. Compared to the virtual preoperative planning, the average linear variation of the osteotomized segments was 1.36±0.4 mm, and the average angular variation was 4.26±1.78°.

3.4 Result of Osteotomy Motion Modeling

The osteotomy motion was modeled by learning from 120 demonstrations three from experienced surgeons. Each surgeon operated on 5 fibulas to harvest 40 FFFs on the platform in Figure 6. Figure 8 shows the result of the EFK of demonstrations and dynamic system generated by the GMM. 10 demonstrations of optical-navigating fibulectomy from intermediate level surgeons were used to compare the performance with robot and experts. Table.1 shows the significant performance differences in manual performances between the experts and intermediate level surgeons. For the robot learning from the expert, the result shows better performance in terms of mean and max speed.

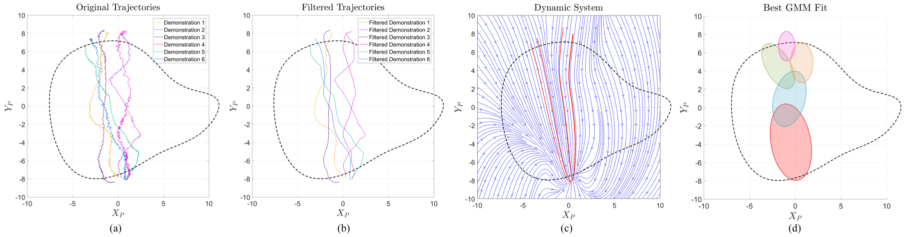

Fig. 8 Unit: mm (a) Original recorded trajectories from experts' manual demonstrations, other demonstrations are not plotted. (b) The filtered trajectories with EKF of demonstrations in (a). (c) The dynamic system. The blue arrows represent the direction of velocity. The red curves are the trajectories generated from demonstration in (a) via GMM. (d) The best GMM fit for all demonstrations with five components. The black dashes in each sub-figure represent one outer boundary of fibula.

Table 1 The cooperation of performance between the osteotomy from robot, intermediate and expert surgeons

Parameters	Robot	Expert	Intermediate
mean speed (mm/s)	0.81	0.76	0.58
max speed (mm/s)	1.08	1.23	1.97

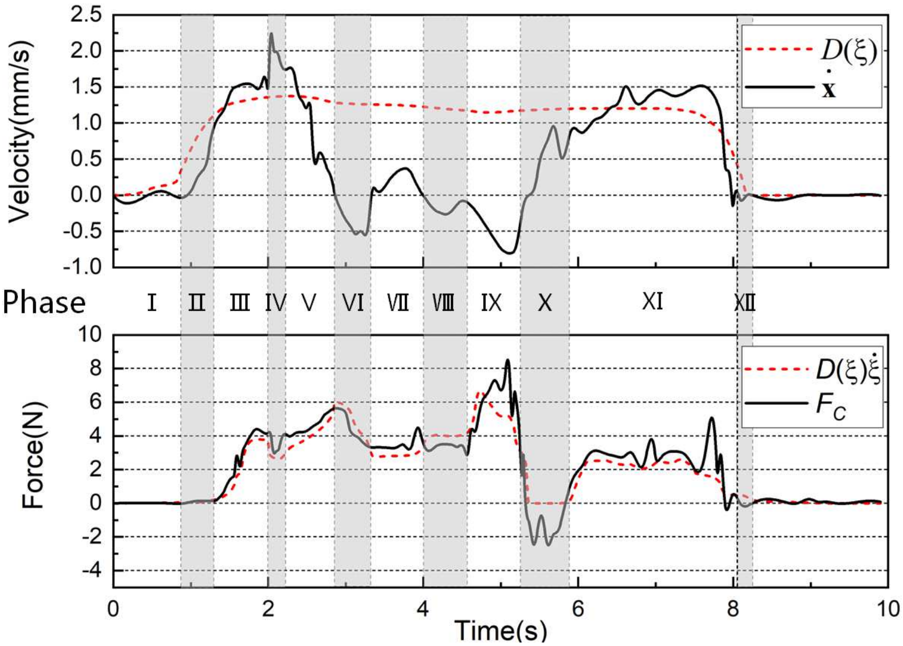

Fig. 9 Upper: The desired velocity in dynamic systems and real velocity of blade. Lower: The threshold force $D(\dot{\xi})\xi$ (red dash curve) and the real force of blade (black curve).

3.5 Result of Sensor-aware Fibular Osteotomy

In order to validate the reliability and robustness of the sensor-aware fibular osteotomy, the experiments were carried out with some external disturbance. Figure 9 shows the results of one typical robot-assisted fibulectomy on our platform.

In this experiment, the fibula model as fibula holder was moved at $t = 2.0$s, and the operator attached force on the saw at $t = 5.25$s. The whole procedure of this robotic-assisted osteotomy could be divided into twelve phases according to the velocity of blade and the cutting force. The first phase ($t = 0 \sim 0.82$s) was preparation, and the osteotomy started at $t = 0.82$s. In the second phase ($t = 0.82 \sim 1.30$s), there was a dramatic increase in the velocity, whereas the force was almost zero, indicating that the saw was moving forward to the entry of planned trajectory. Then, both the velocity and force increased due to the start of cutting during $t = 1.30 \sim 2.88$s. It is worth mentioning that it took about 0.22s ($t = 2.0 \sim 2.22$s) for the robot to adapt to the new target's position (the displacement of the fibula holder is about 10mm). In the sixth ($t = 2.88 \sim 3.37$s) and eighth ($t = 4.01 \sim 4.52$s) phases, the force was below the threshold $\mathbf{D}(\xi)\dot{\xi}$, and velocity was in negative direction accordingly. From $t = 5.25$s to $t = 5.99$s, the $\mathbf{D}(\xi)\dot{\xi}$ was about zero, because the surgical saw was left up by the surgeon and it was at the place where $\mathbf{D}(\xi) = \mathbf{0}$. During $t = 5.99 \sim 7.82$s, the fibula was cut by the blade steadily. Finally, the sawed-through was detected at $t = 7.8$s, where the cutting force was in steep decline. At the same time, the velocity was quickly drop to zeros with overshoot. The terminal threshold $\mathcal{T}$ in sawed-through detection algorithm was set to be 0.5 in this experiment. In the final phase, movement of the end-effector was stopped.

It took about 7 seconds to accomplish a cutting procedure in this example, a bit longer than the average operating time (5.12 ± 1.27s) of 120 robotic-assisted demonstrations, due to the deliberately exerted movement from operator. The mean operation time of manual demonstrations was (7.62 ± 3.71s) in Section 3.2.

3.6 Result of Fibula Sawed-through Detection Algorithm

In the Section 3.5, the dynamic performance of sawed-through detection algorithm was delineated in detail. However, the inevitable overshoot, concerning with the terminal threshold $\mathcal{T}$, in the motion control will pose a threat to the peroneal artery or vein. Moreover, the inappropriate terminal threshold $\mathcal{T}$ will left the fibular bone unsegmented.

In order to determine the suitable $\mathcal{T}$, we first carried out 120 manual trials (same as the trails in Section 3.2) to find an initial range of $\mathcal{T}$, then another 180 robotic-assisted trials were conducted to find the threshold balancing overshoot and the number of unsegmented fibular.

In manual trials, the normalized terminal threshold $\mathcal{T}$ was computed according to (9) and (10). Figure 10(a) shows the distribution of $\mathcal{T}$ in manual

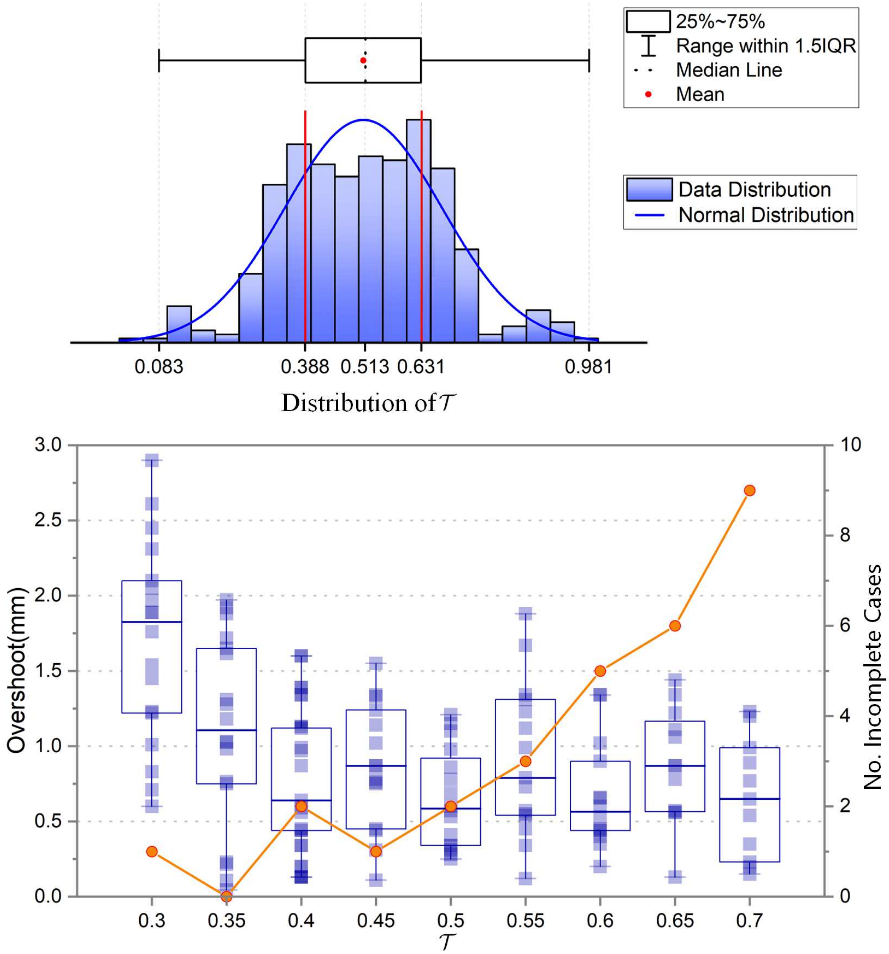

Fig. 10 Upper: The distribution of threshold $\mathcal{T}$ in sawed-through detection algorithm with Gaussian curve. The average is 0.513 with interquartile range(IQR) of $0.388 \sim 0.631$. Lower: The distribution of overshoot (box plots) and the number of incomplete cases (orange line) in experiments with various $\mathcal{T}$.

trails, the average $\mathcal{T}$ is 0.513 with the interquartile range of $0.388 \sim 0.631$, which was regarded as the initial range in robotic-assisted trails.

In robotic-assisted trails, osteotomies were stopped when various $\mathcal{T}$ were achieved. The candidate $\mathcal{T}$ were from 0.3 to 0.7 with equal spacing of 0.05, therefore, each group contains 20 trails. The overshoot was computed via matrix chain in (1) when the robot as well as the blade totally stopped. The results were shown in the Figure 10 (b), the average overshoot of all trails was 0.981mm and the standard deviation was 0.574mm. The minimal average overshoot was 0.65 ± 0.32mm in the fifth group ($\mathcal{T} = 0.5$), whereas the maximal is 1.70 ± 0.65mm ($\mathcal{T} = 0.3$). There are more cases where the cutting is incomplete when the $\mathcal{T}$ increases, especially when $\mathcal{T} = 0.7$, 45% cases were unsuccessful.It can be found that a normalized force threshold value of 0.5 yielded a good balance.

4 Discussion

In the last decade, mandibular reconstruction with FFF in high precision and good safety was a huge challenge for surgeons[27]. Current computer-assisted technologies, such as surgical template, navigation and robot, have further increased the accuracy of surgical outcomes comparing with the freehand surgeries. However, there were many problems concerning with efficiency and safety emerging during the practical clinical applications. To address these problems, we developed a novel robotic platform for sensor-aware fibular osteotomies for mandibular reconstruction surgery. The combination of image-guidance and force feedback provided comprehensive sensing information for a more accuracy and safe osteotomy. These experiments show that this robotic system is suitable for future trials.

Concerning the accuracy of surgical outcomes, the quantitative evaluation showing that the algorithm is able to harvest the expected FFFs. Table 2 compares the accuracy of fibulectomy of different research groups with different computer-assisted surgery technologies. Errors occur in slice thickness, pitch, and algorithm for slice image reconstruction in these aforementioned technologies[28], whereas in robotic-assisted surgery, the error may be attributed to the patient-to-image registration, hand (surgical saw on the end-effector of robot)-eye (optical tracker) calibration, robot control and movement of the fibula holder. In contrast to [15], the cloud point registration applied in our robot system is more precise, because the calibration error was introduced by locating three landmarks in both the real world and the image coordinate system with saw blade tip.

The control of the surgical robot for mandibular reconstruction has been studied before. [16] used the admittance control to realize physical human-robot interaction as well, with which surgeon are able to take advantage of virtual fixture to reach the entry of osteotomy trajectory. However, most of them were focused on the procedure of robotic-assisted positioning rather than osteotomy. To the best of our knowledge, sensor-aware fibula osteotomies we proposed was the first automated and safe control system for intra-operative fibula osteotomy. In hardware, fibula holder have the ability to sense the cutting force equipped with four strain gauges, leading to the circumstance that cutting force could be measured. Therefore, force information could be combined with motion to realize sensor-aware fibular osteotomy. The dynamic system learning from demonstrations of experienced surgeons was able to establish a steady desired velocity field for robot. The robot could imitate fibulectomy from experts to the greatest extent, and have the ability to adapt its trajectory instantly in the face of perturbations. Most importantly, DSAC allows surgeons to have physical interaction with robot during osteotomy, which means surgeons can take over the control of the robot in emergency.

Table 2 Mean Difference Between Planned and Actual Fibular Segment Lengths and Osteotomy Angles in Patients Under-going Mandibular Reconstruction With Computer-Assisted Design and Rapid Prototype Modeling

Method	Author	Year	No. cases	SL mean(mm) $\pm$ SD	SL range(mm)	OA mean($^\circ$) $\pm$ SD	OA range($^\circ$)
Robot-assisted	This study	2021	120	1.08 ± 0.41	$0.23 \sim 2.09$	1.32 ± 0.64	$0.43 \sim 2.94$
	Cheng *et al.*[16]	2020	$18^{\star}$	1.04 ± 0.79	$\diamond$	1.83 ± 0.85	$\diamond$
	Chao *et al.*[17]	2016	$\diamond$	1.3 ± 0.4	$\diamond$	4.2 ± 1.7	$\diamond$
Template-guided	Goormans *et al.*[5]	2019	$\diamond$	$1.74^{\star\star}$	$0.02 \sim 6.10$	$1.98^{\star}$	$0.04 \sim 5.86$
	Zhang *et al.*[6]	2016	8	1.34 ± 1.09	$0.16 \sim 3.75$	2.29 ± 1.19	$0.27 \sim 3.73$
	Schepers *et al.*[7]	2015	7	1.0 ± 1.0	$0 \sim 2.98$	3.0 ± 2.1	$0 \sim 14.15$
	Hanasono *et al.*[8]	2012	18	2.46 ± 2.06	$\diamond$	3.51 ± 2.69	$\diamond$
Navigation-guided	Pietruski *et al.*[29]	2019	$\diamond$	1.85 ± 0.99	$0.71 \sim 5.02$	3.66 ± 3.06	$0.90 \sim 18.69$

SL = segment length; OA = osteotomy angle; SD = standard deviation; $\diamond$ = not mentioned; * tube model; ** the standard deviation was not mentioned

Hybrid force-motion control for contact task has been studied both in industrial (e.g. robotic polishing[30], cutting[31]) and medical applications (e.g. robotic ultrasound acquisition[32]). Some studies use the impedance control to realized human-robot interaction, however, some manipulator without torque sensing ability can only receive high-level position or speed command rather than joint torques. Some studies generate constrained position or velocity real-time to fulfill tasks. Therefore, according to the performance of DSAC in experiments, it could be regarded as a suitable solution to robotic-assisted osteotomy. Moreover, according to the stereotyped decrease in cutting force when the blade saws through the fibular, we proposed a fibula sawed-through detection algorithm. The robotic system utilized this algorithm to perform automated osteotomies with high precision and the ability to stop with 1.50mm resolution when the terminal threshold is 0.5. The mock peroneal artery and vein was not been touched or cut by the saw in the experiments.

The presented robot system has some technical and clinical limitations. In the first place, different kinds of surgical saws, such as reciprocating and oscillating saws, with various operating frequency, have been used in fibular osteotomy. In clinical, the osteotomy trajectory of oscillating saws is longer because of its narrow blade. The control of surgical robot in this study was based on the usage reciprocating saws, especially the modeling of osteotomy motion, may not be simply transfer to the robotic osteotomy system with oscillating saws. Secondly, although the cutting efficiency and accuracy has been raised, comparing with manual operation, the whole procedure is much time-consuming in contrast to free-hand and template-guided osteotomy.

For the autonomy of fibula osteotomy in mandibular reconstruction, our approach is an important first step to turn shared-decision fibular osteotomy into practice. The robot control switches from the human operator to the machine for the duration of the task to be executed. Our surgical robot, of course, do not replace human surgeons, but it should result in more accuracy FFFs with safer osteotomies than previously possible. Furthermore, harvesting FFFs, something that typically requires extensive training, can now be performed by novice surgeons with anatomical knowledge.

5 Conclusion

In this paper, we report the development, control and evaluation of a new robot system for fibula osteotomy in mandibular reconstruction. The surgical robot proposed enables to interact with surgeons during the surgery. Surgeon can locate the surgical saw to planed entry with the help of robot. The hybrid motion-force control has been introduced to risk of vessel rupture led by unexpected over force. During the osteotomy, according to the motion and force, the robot can immediately react the perturbations. Compare with other surgical robot system, the accuracy of our system is higher. Phantom trials were successfully conducted to provide proof of concept for sawed-through detection algorithm. Shared decision, include auto-osteotomy and human-robot collaboration, was studied in our work, and surgeon can easily operative the osteotomy.

In future work, we will use real fibula rather than resin phantom for experiments, and analysis the impact of bone density for sawed-through detection.

Declarations

Acknowledgments. This work was supported by Shanghai Jiao Tong University Foundation on Medical and Technological Joint Science Research (ZH2018ZDA15).

Conflict of interest. The authors declare that they have no conflict of interest.

Ethical approval. The ethics approval of this study is given by Ethics Committee of Shanghai Ninth People's Hospital, Shanghai Jiao Tong University School of Medicine (IRB Number: SH9H-2019-T109-1).

Informed consent. Not applicable.

References

[1] Kokosis, G., Schmitz, R., Powers, D.B., Erdmann, D.: Mandibular reconstruction using the free vascularized fibula graft: An overview of different modifications. Arch Plast Surg **43**(1), 3–9 (2016)

[2] Wilde, F., Cornelius, C.-P., Schramm, A.: Computer-assisted mandibular reconstruction using a patient-specific reconstruction plate fabricated with computer-aided design and manufacturing techniques. Craniomaxillofac Trauma Reconstr **7**(2), 158–166 (2014)

[3] Tsai, M.-J., Wu, C.-T.: Study of mandible reconstruction using a fibula flap with application of additive manufacturing technology. Biomed Eng Online **13**(1), 57 (2014)

[4] Qu, X., Zhen, W., Ong, H.S., Zhang, C., Abdelrehem, A.: Accuracy of computer-aided design/computer-aided manufacturing surgical template for guidance of dental implant distraction in mandibular reconstruction with free fibula flaps. J Craniofac Surg **31**(2), 355–359 (2020)

[5] Goormans, F., Sun, Y., Bila, M., Schoenaers, J., Geusens, J., Lübbers, H.-T., Coucke, W., Politis, C.: Accuracy of computer-assisted mandibular reconstructions with free fibula flap: Results of a single-center series. Oral Oncol **97**, 69–75 (2019)

[6] Zhang, L., Liu, Z., Li, B., Yu, H., Shen, S.G., Wang, X.: Evaluation of computer-assisted mandibular reconstruction with vascularized fibular

flap compared to conventional surgery. Oral Surg Oral Med Oral Pathol Oral Radiol **121**(2), 139–148 (2016)

[7] Schepers, R.H., Kraeima, J., Vissink, A., Lahoda, L.U., Roodenburg, J.L., Reintsema, H., Raghoebar, G.M., Witjes, M.J.: Accuracy of secondary maxillofacial reconstruction with prefabricated fibula grafts using 3d planning and guided reconstruction. J Craniomaxillofac Surg **44**(4), 392–399 (2016)

[8] Hanasono, M.M., Skoracki, R.J.: Computer-assisted design and rapid prototype modeling in microvascular mandible reconstruction. Laryngoscope **123**(3), 597–604 (2013)

[9] Ma, Q., Kobayashi, E., Suenaga, H., Hara, K., Wang, J., Nakagawa, K., Sakuma, I., Masamune, K.: Autonomous surgical robot with camera-based markerless navigation for oral and maxillofacial surgery. IEEE/ASME Transactions on Mechatronics **25**(2), 1084–1094 (2020). https://doi.org/10.1109/TMECH.2020.2971618

[10] Kong, X., Duan, X., Wang, Y.: An integrated system for planning, navigation and robotic assistance for mandible reconstruction surgery. Intell Serv Robot **9**(2), 113–121 (2016)

[11] Wang, Y., Duan, X.: Spatial registration for a three-arm robot assisted mandible reconstruction surgery. Math Probl Eng **2015**, 1–10 (2015)

[12] Chao, A.H., Weimer, K., Raczkowsky, J., Zhang, Y., Kunze, M., Cody, D., Selber, J.C., Hanasono, M.M., Skoracki, R.J.: Pre-programmed robotic osteotomies for fibula free flap mandible reconstruction: A preclinical investigation. Microsurgery **36**(3), 246–249 (2015)

[13] Augello, M., Baetscher, C., Segesser, M., Zeilhofer, H.-F., Cattin, P., Juergens, P.: Performing partial mandibular resection, fibula free flap reconstruction and midfacial osteotomies with a cold ablation and robot-guided er: Yag laser osteotome (carlo®)–a study on applicability and effectiveness in human cadavers. J Craniomaxillofac Surg **46**(10), 1850–1855 (2018)

[14] Ureel, M., Augello, M., Holzinger, D., Wilken, T., Berg, B.-I., Zeilhofer, H.-F., Millesi, G., Juergens, P., Mueller, A.A.: Cold ablation robot-guided laser osteotome (carlo®): From bench to bedside. J Clin Med **10**(3), 450 (2021)

[15] Johansson, R., Santelices, I., O'Connell, D., Tavakoli, M., Aalto, D.: Evaluation of the use of haptic virtual fixtures to guide fibula osteotomies in mandible reconstruction surgery. In: IEEE Int Conf Automation Sci Eng (CASE) (2019)

[16] Cheng, L., Carriere, J., Piwowarczyk, J., Aalto, D., Zemiti, N., de Boutray, M., Tavakoli, M.: Admittance-controlled robotic assistant for fibula osteotomies in mandible reconstruction surgery. Adv Intell Syst **3**(1), 2000158 (2021)

[17] Chao, A.H., Weimer, K., Raczkowsky, J., Zhang, Y., Kunze, M., Cody, D., Selber, J.C., Hanasono, M.M., Skoracki, R.J.: Pre-programmed robotic osteotomies for fibula free flap mandible reconstruction: A preclinical investigation. Microsurgery **36**(3), 246–249 (2016)

[18] Pak, N., Siegle, J.H., Kinney, J.P., Denman, D.J., Blanche, T.J., Boyden, E.S.: Closed-loop, ultraprecise, automated craniotomies. J Neurophysiol **113**(10), 3943–3953 (2015)

[19] Yang, G.-Z., Cambias, J., Cleary, K., Daimler, E., Drake, J., Dupont, P.E., Hata, N., Kazanzides, P., Martel, S., Patel, R.V., *et al.*: Medical robotics-regulatory, ethical, and legal considerations for increasing levels of autonomy. Sci Robot **2**(4), 8638 (2017)

[20] Haidegger, T.: Autonomy for surgical robots: Concepts and paradigms. IEEE Trans Med Robot Bionics **1**(2), 65–76 (2019)

[21] Giovanni, S., Mattia, B., Bruno, B., Pierluigi, T., F, G., P, A., Erika, C.: Step-by-step surgical technique for mandibular reconstruction with fibular free flap: application of digital technology in virtual surgical planning. Eur Arch Otorhinolaryngol **272**, 1491–1501 (2015)

[22] Li, Y., Hu, J., Tao, B., Yu, D., Shen, Y., Fan, S., Wu, Y., Chen, X.: Automatic robot-world calibration in an optical-navigated surgical robot system and its application for oral implant placement. Int J Comput Assist Radiol Surg **15**, 1685–1692 (2020)

[23] Cohn, D.A., Ghahramani, Z., Jordan, M.I.: Active learning with statistical models. J Artif Intell Res **4**, 129–145 (1996)

[24] Khansari-Zadeh, S.M., Billard, A.: Learning stable nonlinear dynamical systems with gaussian mixture models. IEEE Transactions on Robotics **27**(5), 943–957 (2011)

[25] Lee, S., Chung, C.K., Oh, S.H., Park, S.B.: Correlation between bone mineral density measured by dual-energy x-ray absorptiometry and hounsfield units measured by diagnostic ct in lumbar spine. J Korean Neurosurg Soc **54**(5), 384 (2013)

[26] Reif, K., Gunther, S., Yaz, E., Unbehauen, R.: Stochastic stability of the discrete-time extended kalman filter. IEEE Transactions on Automatic control **44**(4), 714–728 (1999)

[27] Yamakawa, S., Hayashida, K.: Safety and efficacy of secondary mandibular reconstruction using a free osteo-cutaneous fibula flap after segmental mandibular resection: a retrospective case–control study. BMC Surg. **21**(1), 1–9 (2021)

[28] van Baar, G.J., Forouzanfar, T., Liberton, N.P., Winters, H.A., Leusink, F.K.: Accuracy of computer-assisted surgery in mandibular reconstruction: a systematic review. Oral oncology **84**, 52–60 (2018)

[29] Pietruski, P., Majak, M., Światek-Najwer, E., Żuk, M., Popek, M., Mazurek, M., Świecka, M., Jaworowski, J.: Navigation-guided fibula free flap for mandibular reconstruction: A proof of concept study. J Plast Reconstr Aesthet Surg **72**(4), 572–580 (2019)

[30] Kronander, K., Billard, A.: Passive interaction control with dynamical systems. IEEE Robot Autom Lett **1**(1), 106–113 (2017)

[31] Jung, S., Hsia, T.C.: Adaptive force tracking impedance control of robot for cutting nonhomogeneous workpiece. In: IEEE Int Conf Robot Autom(ICRA), vol. 3, pp. 1800–1805 (1999). IEEE

[32] Jiang, Z., Grimm, M., Zhou, M., Hu, Y., Esteban, J., Navab, N.: Automatic force-based probe positioning for precise robotic ultrasound acquisition. IEEE Transactions on Industrial Electronics (2020)